7.1 DEVELOPMENT OF A FINE SCALE SMOKE DISPERSION MODELING SYSTEM. PART II - CASE STUDY OF A PRESCRIBED BURN IN THE NEW JERSEY PINE BARRENS

MICHAEL T. KIEFER*[1], WARREN E. HEILMAN[2], SHIYUAN ZHONG[1], JOSEPH J. CHARNEY[2], XINDI BIAN[2], RYAN P. SHADBOLT[1], JOHN L. HOM[4], KENNETH L. CLARK[3], NICHOLAS SKOWRONSKI[3], MICHAEL GALLAGHER[3], AND MATTHEW PATTERSON[4]
[1]Michigan State University, East Lansing, Michigan
[2]USDA Forest Service, Northern Research Station, East Lansing, Michigan
[3]USDA Forest Service, Northern Research Station, New Lisbon, New Jersey
[4]USDA Forest Service, Northern Research Station, Newtown Square, Pennsylvania

1. INTRODUCTION

Smoke dispersion from wildland fires is a critical health and safety issue, impacting air quality and visibility across a broad range of space and time scales. Predicting the dispersion of smoke from low-intensity fires is particularly challenging due to the fact that it is highly sensitive to factors such as near-surface meteorological conditions, local topography, vegetation, and atmospheric turbulence within and above vegetation layers. Prescribed fires are useful tools for forest ecology and management and generally are low in intensity, confined to small areas, and capable of producing smoke that may linger in an area for extended periods of time. Existing integrated smoke dispersion modeling systems, which are designed for predictions of smoke from multiple sources on a regional scale [e.g., BlueSky (Larkin et al., 2009)], do not have the necessary resolution to accurately capture smoke from low-intensity fires that tends to meander around the source and may stay underneath forest canopies for a relatively long period of time. Simple dispersion models [e.g., SASEM, VSMOKE (Riebau et al., 1988; Lavdas, 1996)], which typically are location specific, are limited by their simplistic nature in treating the emissions source, topography, canopy, and the atmospheric conditions.

In order to model smoke dispersion within a forest canopy as well as possible transport of smoke through the canopy - free atmosphere interface and into the planetary boundary layer, use of a large-eddy simulation (LES) model is essential. However, application of LES to simulation of flow inside a forest canopy requires that the effects of the canopy on air flow be accounted for. In this paper, we describe the application of a newly developed canopy flow modeling system, based on the Advanced Regional Prediction System (ARPS) (Xue et al., 2000, 2001), to simulation of the meteorology near a prescribed burn inside the Pine Barrens of southern New Jersey. Flux towers fitted with a variety of instrumentation (e.g., sonic anemometers, thermocouples) collected meteorological data during the experiment (Fig. 1a); meteorological data from a 20-m flux tower are utilized for model validation purposes here. Validation of the model results are presented for the burn day (20 March 2011) and the previous day when data were collected but no burning was conducted (19 March 2011).

2. MODEL DESCRIPTION

a. Modifications made to ARPS

The need for a modeling system capable of simulating mean and turbulent components of flow through a canopy under all stability regimes, including regimes generated by wildland fires, motivated the following additions to the ARPS model equations and parameterization routines. Following Dupont and Brunet (2008), we have added a term to the momentum equation to account for pressure and viscous drag that occurs due to the presence of the canopy elements, and a term to the subgrid-scale (SGS) turbulent kinetic energy (TKE) equation to account for the enhancement of turbulence dissipation in the canopy air space. Following Kanda and Hino (1994), we have also added a production term to the SGS TKE equation to represent the production of SGS TKE in the wakes of canopy elements, at scales large enough that the turbulence does not dissipate immediately yet small enough that it remains unresolved.

Regarding the impact of the canopy elements on heating/cooling processes inside the canopy layer, we follow Sun et al. (2006) and make the following modifications. First, we modify the radiation physics subroutine to compute net radiation flux at canopy top and prescribe a profile of net radiation that produces an approximately exponential decay within the canopy. Second, a term is added to the thermodynamic equation to represent heating/cooling of the canopy air spaces that results from the vertical flux divergence of canopy net radiation. Lastly, the ARPS surface physics subroutine is modified such that ground net radiation flux is attenuated before calls to the soil-vegetation subroutine are made. A detailed de-

Corresponding author address: Michael Kiefer, Department of Geography, Michigan State University, 116 Geography Building, East Lansing, MI 48823.
E-mail: mtkiefer@msu.edu

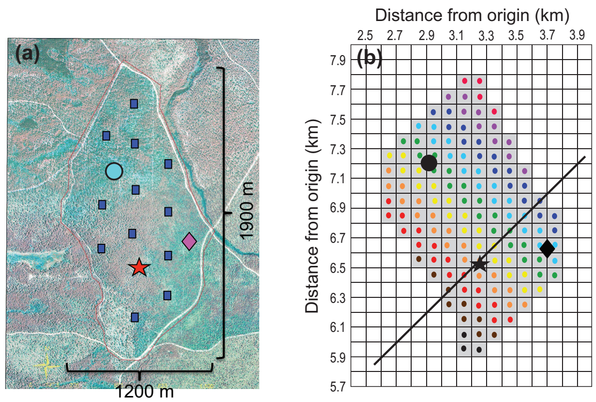

Figure 1: Overview of the burn unit with locations of instrumented towers: (a) aerial image of burn unit and (b) schematic of model burn unit. Towers are denoted by symbols: square - 3-m tower; circle- 10-m tower; star - 20-m tower; diamond - 30-m tower. Circles in (b) denote grid points inside the burn unit; colors denote "burn zones" in which a common start time, peak time, end time, and fire intensity are specified based on heat flux measurements from the flux towers. Thick line in (b) indicates cross section axis used in Fig. 3.

scription of the various modifications made to the ARPS model may be found in the companion paper presented at this meeting (Part I; Kiefer et al., 2011).

In addition to the canopy modifications made to ARPS, a relatively simple fire parameterization has been adopted. The fire is implemented in the model by prescribing surface heat fluxes at specified grid points in the model during a fixed time period. As Fig. 1b depicts, the burn unit is depicted in the model as an irregularly shaped group of grid cells in the northwest quadrant of the model domain. Note that the geographic coordinates of the center of the burn unit in the model match the actual coordinates of the burn unit center (Fig. 1a). The simulated burn unit is divided in the model into ten burn zones inside which each grid cell shares a common fire start, peak, and end time, and maximum fire intensity. One equation with a cubic function is used to quickly ramp up the surface heat flux from start time to peak time, and another function is used to gradually ramp the flux down from the peak time to end time. The model fire parameters (e.g., start time, peak intensity) are based on measurements from the instrumented towers (see symbols in Fig. 1a). The simulated burn zones are ignited from southwest to northeast, following as closely as possible the observed ignition timing. However, it is important to note that the fire spread pattern we adopt in the model is an approximation of the more complicated actual fire spread pattern.

b. Model Configuration

To accurately represent regional and local forcing within the area of the burn site, a series of 5 one-way nested simulations are executed, spanning from 8100-m to 100-m horizontal grid spacing with a 1:3 nesting ratio. For reference, the outer grid covers the northeastern United States from Virginia northward and from eastern Ohio eastward, and the innermost domain covers a 100 km^2 area surrounding the burn unit. Simulations conducted include four outer-grid simulations (8100, 2700, 900, and 300 m horizontal grid spacing), initialized at 0000 UTC 19 March 2011 and run for 60 hours, and two 12-hour inner-grid simulations, initialized at 1200 UTC 19 March (pre-burn case) and 1200 UTC 20 March (burn case). North American Regional Reanalysis (NARR) (Mesinger et al., 2006) data is used to specify both initial and boundary conditions for the outermost grid. Land use and terrain data are input from the U.S. Geological Survey (USGS) 1-km and 100-m datasets, respectively. Stretching is applied along the vertical axis in all simulations, with 2-m vertical grid spacing in the lowest 84 m of the atmosphere in the innermost grid. The canopy is applied to the innermost nest only, wherein the bulk effect of the canopy is represented by frontal area density (one-sided leaf area per unit volume; m^2 m^{-3}). In order to provide the canopy modeling system with vegetation density information, a three-dimensional frontal area density dataset, derived from canopy lidar measurements, is utilized.

3. RESULTS AND DISCUSSION

a. 19 Mar 2011: Pre-burn case

To assess the performance of the canopy modeling system without heat output from the fire, vertical profiles of simulated 3-hour mean TKE, wind speed and direction, and temperature (averaged over 3 grid points adjacent to the 20-m tower location) are presented in Fig. 2, with corresponding flux tower data overlaid. For 3-hour mean TKE (Fig. 2a), the model is found to under-predict turbulence inside the canopy, but exhibit only about 8% error just above the canopy at 20 m above ground level. It is important to note that the "S"-shaped TKE profile agrees favorably with results from previous LES modeling studies in neutral boundary layers (Shaw and Schumann, 1992; Shaw and Patton, 2003; Dupont and Brunet, 2008). Regarding mean wind speed (Fig. 2b), the model profiles show agreement with the observations, although wind speeds are underestimated inside the canopy and overestimated in the free air above. However, the simulated wind direction is found to deviate considerably from observations at all levels in and above the canopy. Mean wind direction above the canopy is approximately

325 degrees (NW), compared to 350 degrees (N) as measured by the sonic anemometer at the 20 m level. The wind direction bias is likely related to a tendency of ARPS to move an area of surface high pressure offshore in the outer-grid simulations too slowly compared to observations (not shown). The near-surface mean wind in the burn unit shifts gradually from 325 to 350 degrees in the ARPS simulation, but this shift occurs later in the day than in reality. Lastly, examining simulated mean temperature (Fig. 2c), an overly strong superadiabatic layer is evident. It is worth noting that although surface temperatures are too warm compared to the observations, the simulated lapse rates in and above the canopy show good agreement with the thermocouple measurements.

b. 20 Mar 2011: Burn case

We next consider the simulated wind and temperature structure above the parameterized fire by examining vertical cross sections through the burn zone at 1524 EDT (Fig. 3). The burn zone in the model at this time is depicted by the orange shaded circles in Fig. 1b, within which the approximate position of the 20-m flux tower is indicated by the star symbol. In Fig. 3a, it can be seen that the model produces a plume of warm air tilted toward the northeast. The ambient wind direction varied between east-northeast and east-southeast during the day, thus the plume in Fig. 3a is tilted into the ambient wind. Examining horizontal wind speed and direction in Fig. 3b, one can see the impact of the fire heat source on the wind field inside the canopy (i.e. below 18 m AGL). An area of relatively strong southwest winds on one side of the warm plume and lighter east winds on the other side (Fig. 3b) are indicative of an inflow circulation. The simulated plume orientation and wind field anomaly qualitatively agrees with the observations, as evidenced by the temperature and wind component timeseries measured by the sonic anemometer, as seen in Fig. 4. In Fig. 4a, the spike of warm air associated with the fire front around 20.8 UTC arrives first at the 20-m level, followed in sequence by the 10- and 3-m levels. Given the fact that the fire front was approaching from the southwest, this implies that the column of warm air above the fire was tilted from vertical with a qualitatively similar orientation to the simulated plume. Additionally, the horizontal wind component timeseries in Fig. 4b indicates a pronounced wind shift from light easterly prior to 20.8 UTC to southwest winds of 2-3 m s^{-1} during the time of the fire front passage.

4. CONCLUSIONS

The preliminary validation efforts presented here have shown that the ARPS model is able to reproduce many

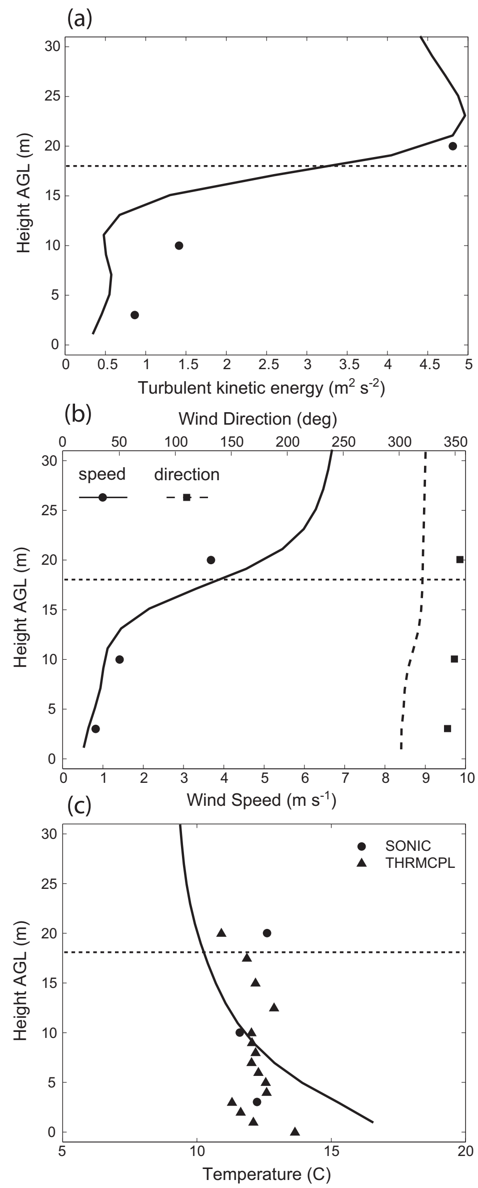

Figure 2: Vertical profiles of 3-hour mean (1430-1730 EDT) simulated (a) turbulent kinetic energy (m^2 s^{-2}), (b) wind speed (m s^{-1}), and (c) temperature (C) for 19 March 2011 pre-burn case. Observed values from 20-m tower are denoted by symbols (circles, squares: sonic anemometer; triangles: thermocouple). Total simulated TKE (resolved + subgrid-scale) is displayed in this and all subsequent figures. Note that simulated profiles are also averaged spatially around tower location (3-point average). The canopy top is indicated by a horizontal dotted line in each panel.

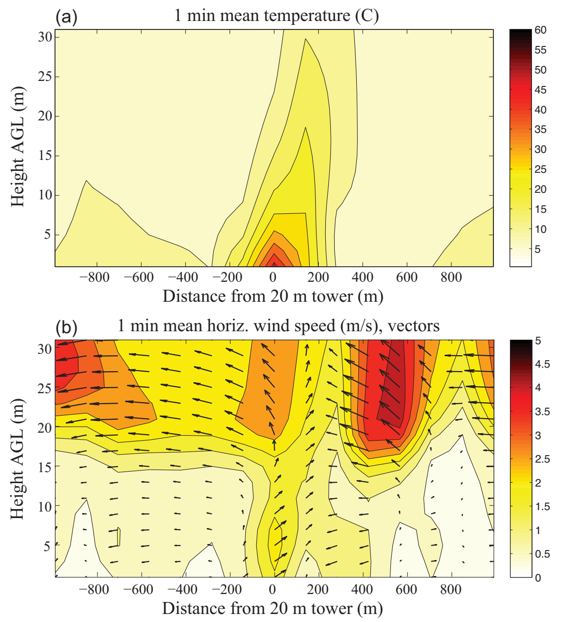

Figure 3: Vertical cross section of simulated 1-min mean (a) temperature and (b) horizontal wind speed and direction, at 1524 EDT 20 March. Cross section extends approximately 1 km upstream of the 20-m tower location to 1 km downstream. Contour interval in (a) is 5 degrees C and in (b) is 0.5 m s^{-1}.

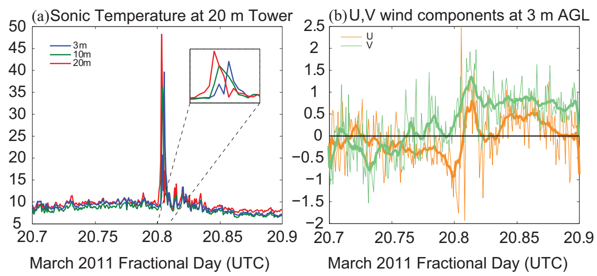

Figure 4: Timeseries of sonic-anemometer observed 1-min mean (a) temperatures (°C) and (b) U- and V- wind components (m s^{-1}) at the 3-m level, between 20.7 and 20.9 March 2011 fractional day (UTC) [i.e., between 1248 and 1736 EDT 20 March 2011]. Inset panel is included in (a) in order to better visualize the approximately 15 minute period during which the fire front passed the 20-m tower. Thick lines in (b) depict 15-min moving averages of the two wind components.

aspects of the observed mean profiles on the pre-burn day (19 March), including mean TKE near the canopy top and mean thermal stratification in and above the canopy. For the simulation with a parameterized fire, plume cross-sections revealed a plume tilted into the ambient wind, and an inflow circulation dominated by a southwest wind field considerably stronger than the ambient flow inside the canopy. Such aspects of the heated plume and fire-scale circulation were shown to be in qualitative agreement with the flux tower observations.

We wish to reiterate here that these results are preliminary. Ongoing work includes further refinement of the fire parameterization (e.g., surface heat flux, timing), computing a budget of resolved TKE, and revising the model code to make the fire parameterization more user-flexible. Furthermore, meteorological data from ARPS (e.g., wind velocity, TKE) is an essential input for the particle dispersion model chosen for this study, the Pacific Northwest National Laboratory (PNNL) Integrated Lagrangian Transport (PILT) model [a recently revised version of the FLEXPART model (Fast and Easter, 2006)]. Results from the PILT simulations will in turn be validated against $PM_{2.5}$ measurements from an array of towers implemented during the burn experiment. The lack of research on smoke transport from low-intensity fires and the lack of operational modeling tools for predicting smoke dispersion within and in the vicinity of forest vegetation layers makes this work particularly relevant and motivates further efforts.

ACKNOWLEDGMENTS

Support for this research was provided by the U.S. Joint Fire Science Program (Project #9-1-04-1) and the USDA Forest Service (Research Joint Venture Agreement #09-JV-11242306-089). The experimental burn was conducted by the New Jersey Forest Fire Service. We wish to thank Jovanka Nikolic and Wei Lu for reviewing a draft of this paper and providing helpful comments and suggestions.

REFERENCES

Dupont, S., and Y. Brunet, 2008: Influence of foliar density profile on canopy flow: A large-eddy simulation study. *Agric. For. Meteorol.*, **148**, 976–990.

Fast, J. D., and R. C. Easter, 2006: A Lagrangian particle dispersion model compatible with WRF. Preprints, *Seventh Annual WRF User's Workshop*, Boulder, CO.

Kanda, M., and M. Hino, 1994: Organized structures in developing turbulent flow within and above a plant canopy, using a large eddy simulation. *Bound.-Layer Meteor.*, **68**, 237–257.

Kiefer, M. T., S. Zhong, W. E. Heilman, J. J. Charney, X. Bian, and R. P. Shadbolt, 2011: Development of a fine scale smoke dispersion modeling system. Part I: Validation of the canopy model component. *Proc. 9th Symposium on Fire and Forest Meteorology*, Palm Springs, CA, Amer. Meteor. Soc. Extended Abstract

Larkin, N. K., S. M. O'Neill, R. Solomon, S. Raffuse, T. Strand, D. C. Sullivan, C. Krull, M. Rorig, J. L. Peterson, and S. A. Ferguson, 2009: The BlueSky smoke modeling framework. *Int. J. Wildland Fire*, **18**, 906–920.

Lavdas, L., 1996: Program VSMOKE - User's manual. USDA Forest Service, Gen. Tech. Report SRS-6, 156 pp.

Mesinger, F., G. DiMego, E. Kalnay, K. Mitchell, P. C. Shafran, W. Ebisuzaki, D. Jovic, J. Woollen, E. Rogers, E. H. Berbery, M. B. Ek, Y. Fan, R. Grumbine, W. Higgins, H. Li, Y. Lin, G. Manikin, D. Parrish, and W. Shi, 2006: North American Regional Reanalysis. *Bull. Amer. Meteor. Soc.*, **87**, 343–360.

Riebau, A. R., D. G. Fox, M. L. Sestak, B. Dailey, and S. F. Archer, 1988: Simple approach smoke estimation model. *Atmos. Environ.*, **22**, 783–788.

Shaw, R. H., and E. G. Patton, 2003: Canopy element influences on resolved- and subgrid-scale energy within a large-eddy simulation. *Agric. For. Meteorol.*, **115**, 5–17.

Shaw, R. H., and U. Schumann, 1992: Large-eddy simulation of turbulent flow above and within a forest. *Bound.-Layer Meteor.*, **61**, 47–64.

Sun, H., T. L. Clark, R. B. Stull, and T. A. Black, 2006: Two-dimensional simulation of airflow and carbon dioxide transport over a forested mountain. Part I: Interactions between thermally-forced circulations. *Agric. For. Meteorol.*, **140**, 338–351.

Xue, M., K. K. Droegemeier, and V. Wong, 2000: The Advanced Regional Prediction System (ARPS) – A multi-scale nonhydrostatic atmosphere simulation and prediction model. Part I: Model dynamics and verification. *Meteor. Atmos. Phys.*, **75**, 463–485.

Xue, M., K. K. Droegemeier, V. Wong, A. Shapiro, K. Brewster, F. Carr, D. Weber, Y. Liu, and D. Wang, 2001: The Advanced Regional Prediction System (ARPS) – A multi-scale nonhydrostatic atmosphere simulation and prediction tool. Part II: Model physics and applications. *Meteor. Atmos. Phys.*, **76**, 143–165.